Accepted for Soil Dynamics & Earthquake Engineering 14 February 2018

Mapping the uncertainty in modulus reduction and damping curves onto the uncertainty of site amplification functions

Mahdi Bahrampouri[a], Adrian Rodriguez-Marek[a]*, and Julian J. Bommer[b]

a) Charles E. Via, Jr. Department of Civil and Environmental Engineering, Virginia Tech, Blacksburg, VA 24061, USA.
b) Civil and Environmental Engineering, Imperial College London, London SW7 2AZ, U.K.
* Corresponding Author

ABSTRACT

Probabilistic seismic hazard analysis often requires the use of site response analyses to calculate site amplification factors (AFs) that capture the effects of near-surface layers. The site response analyses must also be conducted in a probabilistic framework to quantify the variability in AFs resulting from variation in the rock input motions and uncertainty in the dynamic properties of the soil profile, including uncertainty in the shear-wave velocity and in the nonlinear behavior of the soil. In equivalent linear analyses, the latter is captured through modulus reduction and damping curves (MRD). The joint randomization of shear-wave velocity and MRD curves can result in large computational costs. The objective of this paper is to propose a procedure to separately calculate the contribution of uncertainty in the MRD curves to the total uncertainty in the AFs for a site. This procedure is illustrated in an application for a seismic hazard and risk assessment of the Groningen gas field in the Netherlands. The results show that the effect of uncertainty in MRD curves on the uncertainty in the AFs is highly dependent on soil profile. This effect can be significant for soft soils and strong input motions. Results also indicate that the effects of MRD uncertainty can be correlated to elastic site properties.

Keywords: Probabilistic seismic hazard assessment, site response, site amplification, modulus reduction and damping curves

1. Introduction

Within state-of-practice probabilistic seismic hazard analyses (PSHA) for the sites of safety-critical structures it is not generally considered adequate to represent local site effects through the use of generic amplification terms in ground motion prediction equations (GMPEs) conditioned on parameters such as the time-averaged shear-wave velocity over the uppermost

30 meters, V_{S30}. Instead, the hazard is calculated at a buried reference rock horizon and then combined with site amplification factors (AFs; defined as the ratio of spectral acceleration at the surface over spectral acceleration of the input motion at the reference rock horizon) specific to the overlying profile up to the target horizon at the site (*e.g.*, Bazzurro and Cornell [1]; Rodriguez-Marek *et al.* [2]). In order for the probabilistic nature of the hazard estimates to be retained, and indeed to correctly determine the annual exceedance frequency of the surface motions, the site response analyses performed to calculate the local AFs must also be probabilistic, capturing the variability in AF due to variation in the rock input motions and in the dynamic properties of the soil profile (Bazzurro and Cornell [3]).

Factors whose uncertainty should be incorporated into the calculation of AFs include both the input motions at the reference rock horizon and the parameters that define the dynamic characteristics of the overlying soil profile. To capture motion-to-motion variability, site response analyses are repeated for multiple inputs at each intensity level in order to capture the influence of variation of other characteristics of the motion such as response spectral shape and duration or number of cycles. To capture the uncertainty and variability in the dynamic characteristics of the soil profile, the primary randomization is of the shear-wave velocity (V_S) profile. Low-strain soil damping may also be varied but mass density is usually held constant since the uncertainty in this parameter is generally very small. The other source of variability is that associated with the models for nonlinear soil response, namely the modulus reduction and damping (MRD) curves that define the variation of shear modulus and damping with shear strain in the soil. In order to capture adequately the motion-to-motion variability, and the variability in V_S profiles and MRDs, without giving undue influence to randomly-selected combinations of more extreme values, can require very large numbers of site response analyses. In order to render the calculations more efficient, it is not uncommon to estimate the contribution of uncertainty in MRD curves to the variability in the AFs independently, and only randomize the V_S profiles when performing the site response calculations with the full suite of input motions.

The focus of this paper is to propose a transparent procedure to separately calculate and incorporate the contribution of uncertainty in the MRD curves to the total uncertainty in the AFs for a site. To illustrate the procedure, we present its application to the site response model for the Groningen gas field in the Netherlands where hydrocarbon production is leading to induced earthquakes, in response to which a comprehensive seismic hazard and risk assessment is being undertaken (Bommer *et al.* [4]). A component of the hazard model is a site response model for the entire Groningen field (Rodriguez-Marek *et al.* [5]). This site response model is intended to model the amplification factors (AFs) from the selected reference horizon to the ground surface across the entire field. Since this model is used within a hazard and risk framework, the median and the uncertainty of the AFs must be considered. The uncertainty of the AFs has multiple sources: motion-to-motion variability, uncertainty in shear-wave velocity (V_S) profile, and uncertainty in nonlinear behavior of soil. The uncertainty in the AFs in the Rodriguez-Marek *et al.* [5] study included the effects of motion-to-motion variability and uncertainty the V_S profiles, while the effects of the nonlinear behavior of the soil were borrowed from previous studies. In this study, we present an analysis of the contribution of nonlinear behavior of soil uncertainty on both the median and the uncertainty of AFs for the Groningen field.

Rodriguez-Marek *et al.* [5] used equivalent linear analyses to compute the effects of V_S profile uncertainty and motion-to-motion variability into nonlinear AFs via a Monte Carlo simulation approach, using deterministic modulus reduction and damping (MRD) curves. This approach implies a large number of simulations which are needed to obtain stable estimates of uncertainty. While the same Monte Carlo approach can be used to model the effects of MRD uncertainty on nonlinear AFs, the computational effort is large. Instead, our approach is to develop a model for the contribution of MRD uncertainty by performing rigorous analyses for a representative number of profiles and then we generalize these results by correlating this uncertainty contribution to site parameters. We also propose the use of a sampling technique to minimize the number of simulations needed to obtain stable results.

Following this introduction, the paper begins with a summary of the methodology used in this study along with a summary of previous studies that address the effects of MRD uncertainty on site response estimates. The methodology for the analysis is presented next, including a discussion of the profiles, input motions, and MRD curves used in the study. We then present the results of MRD uncertainty for a representative set of profiles. The results from the site response analyses are then used to develop equations that quantify the effect of uncertainty in MRD on the standard deviation of AFs for the Groningen field.

2. Methodology

2.1 Background and past work

Several studies have estimated the uncertainty in AFs when MRD curves are uncertain. Rathje *et al.* [6] estimated the standard deviation of AFs that results from varying MRD curves while keeping the V_S profile constant and using a given input motion. These authors included four sets of randomized MRD curves and assumed no correlation of MRD curves from layer to layer. They computed values of standard deviation of AF ranging from 0.2 to 0.4 at short periods, and much smaller values at long periods (note that we use a natural logarithmic scale for standard deviation throughout the paper). Kwok *et al.* [7] performed similar analyses on the Turkey Flat site by including three sets of MRD curves with full correlation between layers and found values ranging from 0.1 to 0.2 at short periods and very small values at long periods. Li and Assimaki [8] analyzed two sites in La Cienega using more than 50 MRD curve realizations and using a correlation coefficient of 0.15 between layers for nonlinear soil properties. For the first site, they computed standard deviation values of AFs due to varying MRD curves ranging from 0.3 and 0.4 at short periods and 0.2 at long periods. For the second site, they computed values close to 0.1 at short periods and very small values at long periods. Clearly, the estimated standard deviations of AFs due to randomizing MRD curves vary significantly from study to study. This is partly because of the strong site-dependency of the effects of MRD on site response, and partly because these studies accounted in different ways for the correlations between the different sources of uncertainty. The work presented here presents a systematic approach to capture the effects of MRD uncertainty on the AFs using the Groningen gas field as an example application.

The Groningen gas field is located in the north part of the Netherlands and covers a region about 50 km x 40 km in extension. The region is a flat, low-lying area with thick (over 800 m thick) unconsolidated deposits of Paleogene and Neogene age overlying a much stiffer Cretaceous layer [9]. Near-surface deposits are generally soft Quaternary deposits with average V_S over the upper thirty meters (V_{S30}) lower than about 280 m/s over the entire region. A complete description of the geological and geotechnical characteristics of the region is given in Kruiver *et al.* [9]. The ground motion model for the Groningen gas field is described in detail in Bommer *et al.* [4] and Rodriguez-Marek *et al.* [5]. The model consists of a ground motion prediction equation for a reference rock horizon with a V_S of 1490 m/s. The average depth of this horizon is 800 m, but this depth varies across the field. Site response is accounted for via period-dependent nonlinear AFs. The AFs are computed using site profiles that are built using a geostatistical model for the entire field (Kruiver *et al.* [9]). This model outputs randomized V_S profiles for 100 m by 100 m cells over the entire field. These V_S profiles are used along with input motions generated using a stochastic model to compute AFs for each of the cells. For application, the computed AFs are grouped into 160 zones based on geological considerations and on the similarity in their site response (Fig. 1). The average V_{S30} for each zone is also shown in Fig. 1. Observe that in general the northern portion of the Groningen gas field has softer near-surface soils reflecting a preponderance of intertidal Holocene deposits of fine sands, silts, and clays, with distinct peat layers found in various locations. The surface geology of the southern portion of the field is dominated by somewhat stiffer late Pleistocene deposits of fluvial, glacial, and marine origin, including clays, sands, and some gravels. For each zone, the computed AFs are used to obtain parameters of a period- and intensity-dependent model for the median AF and the standard deviations of the AF for the zone. The standard deviation is meant to account for the spatial variability of the site response within each zone and for the epistemic uncertainty of site properties.

The effects of the variability of site properties and input motion on site response (*e.g.*, on the AFs) are generally captured using a simulation approach, whereas multiple realizations of each of the input parameters are used to compute the statistics of the AFs. Multiple levels of randomization, however, can be computationally expensive. To avoid having to conduct multiple levels of randomization, we assume that the uncertainty due to V_S and input motion variability can be computed separately from that due to MRD uncertainty. This approach is similar to that adopted by Rodriguez-Marek *et al.* [5] for the analysis of site response in the Groningen field. We assume a simple model to incorporate this uncertainty into the uncertainty in AFs:

$$\sigma = \sqrt{\left(\sigma_{GM,V_S}\right)^2 + (\phi_{MRD})^2} \tag{1}$$

where σ denotes the total uncertainty in the logarithm of the AF (for simplicity, we avoid the more cumbersome notation σ_{lnAF}), σ_{GM,V_S} denotes the uncertainty in the logarithms of AF when accounting only for V_S and input motion variability, and ϕ_{MRD} is the additional standard deviation that must be added to account for MRD uncertainty. The value of ϕ_{MRD} must incorporate the effects of the correlation between the different sources of uncertainty, as will be further explained in later sections. Using this notation, the objective of the paper can be restated as the development of a methodology for computing ϕ_{MRD}.

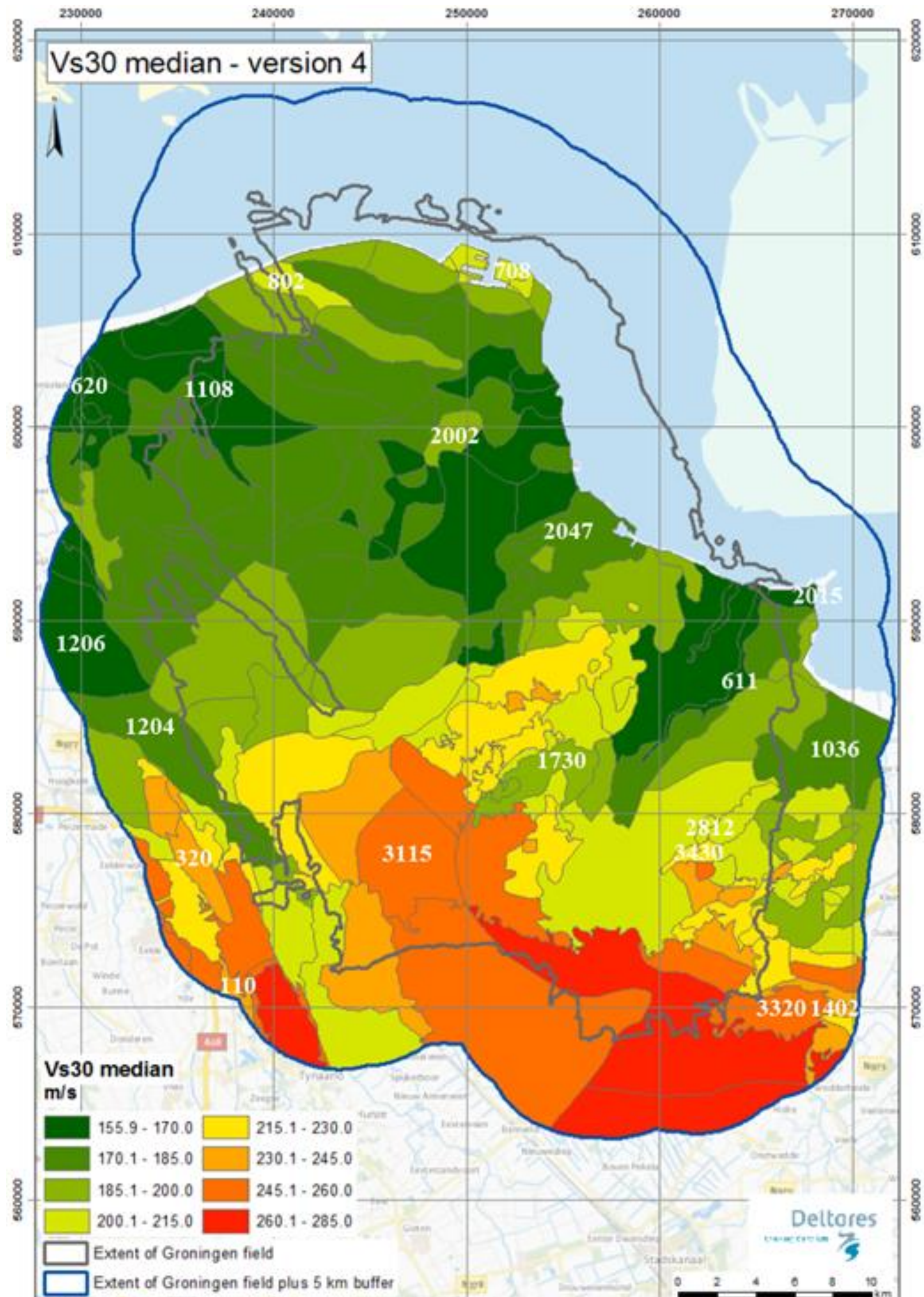

Fig. 1: Median V_{S30} values for each of the zones in the Groningen region (modified from Kruiver *et al.* [9])

2.2 Methodology

We use the site response at a Groningen field as an example of the proposed methodology to compute the effects of MRD uncertainty on the uncertainty in site response. The AFs computed for a given zone are used to develop a period- and intensity-dependent model. These AFs are separated into a median ($\overline{\ln[AF(T)]}$) and a residual (Δ_{AF}). We use the functional form proposed by Stewart *et al.* [10] to model the intensity dependence of the median AFs:

$$\overline{\ln[AF(T)]} = f_1 + f_2 \ln\left(1 + \frac{S_{a,ROCK}(T)}{f_3}\right) \tag{2}$$

where $S_{a,ROCK}(T)$ is the input spectral acceleration at the same oscillator period, and f_1, f_2, and f_3 are period-dependent regression parameters. For simplicity, the (T) representing oscillator period dependence is omitted in the reminder of this paper. The parameters of Eq. (2) have physical interpretations: f_1 corresponds to linear amplification, f_2 is the slope of $ln(AF)$ versus $S_{a,Rock}$ for the nonlinear portion of the curve, and f_3 is approximately the input spectral acceleration at which nonlinearity begins. The residual Δ_{AF} corresponds to the difference between computed AFs for a given combination of input motion and site profile and the median prediction for a given zone, and is assumed to be normally distributed with standard deviation σ. For the Groningen field sites, the standard deviation was observed to vary with input spectral acceleration, which is not unexpected since the influence MRD uncertainty logically increases with the degree of nonlinearity. We use the same model as Rodriguez-Marek *et al.* [5] to capture this variation:

$$\sigma = \begin{cases} \sigma_1 & S_{a,Rock} < S_{a1} \\ \sigma_1 + \dfrac{S_{a.Rock} - S_{a1}}{S_{a,Rock} - S_{a1}}(\sigma_2 - \sigma_1) & S_{a1} < S_{a,Rock} < S_{a2} \\ \sigma_2 & S_{a,Rock} > S_{a2} \end{cases} \tag{3}$$

where σ_1 and σ_2 are model parameters that describe the standard deviation for low-intensity motions ($S_{a,Rock} \le S_{a1}$) and high-intensity motions ($S_{a,Rock} > S_{a2}$), respectively. The parameters of Eqs. (2) and (3) were obtained using maximum likelihood regression for all the zones in the Groningen field (Rodriguez-Marek *et al.* [5]). The threshold accelerations S_{a1} and S_{a2} reflect acceleration levels where the standard deviation of the AF residuals changes behavior. These parameters were obtained from regression analyses of selected zones, and were then set to be constant for the entire field (Rodriguez-Marek *et al.* [5]). An example of these fits for a single oscillator period for Zone 620 in the Groningen field is shown in Fig. 2. This zone is located in the northwest portion of the Groningen field and corresponds to a zone with a V_{S30} value (V_{S30}=193 m/s) that is about average for the Groningen field (Fig.1). Fig. 2 includes AFs computed for all possible combinations of 108 input motions and 50 randomized V_S profiles.

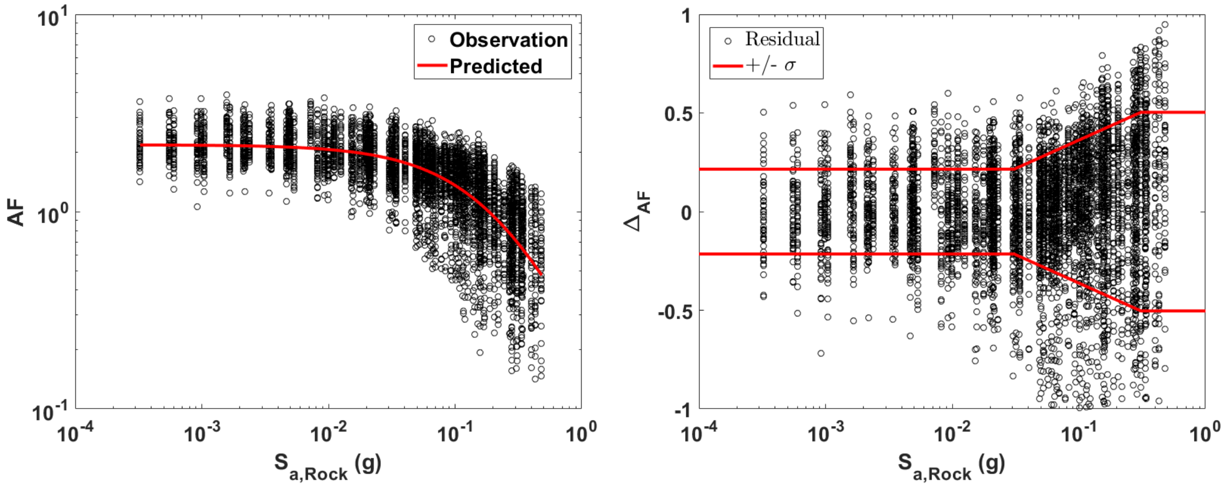

(a) (b)

Fig. 2: (a) Scatter plot of observed AFs (T=0.15s) for zone 620 when the rock input motion and the V_S profile are varied. The red line is the fitted curve (b) Scatter plot of residual AFs (T=0.15s). The red lines show plus and minus one sigma

The standard deviation parameters (σ_1 and σ_2) from Eq. (3) depend on which are the parameters that are randomized in the site response analyses. We assume that the residual Δ_{AF} can be separated into the contributions of each of the sources of uncertainty:

$$\Delta_{AF} = E_{GM} + E_{V_S} + E_{MRD} \tag{4}$$

where Δ_{AF} is the total residual, and E_{GM}, E_{V_S}, and E_{MRD} correspond to the deviation from the mean response resulting from varying only the input motions, the V_S profile, and the MRD curves, respectively. Note these residual terms are mutually dependent. For example, when a soft V_S profile realization is used, varying the MRD curves has a different effect from the cases when a stiff V_S profile is used. The straightforward path for calculating the standard deviation of the total residual (σ) is varying all three input parameters simultaneously and obtaining σ using Eqs. (2) and (3). However, this method is computationally expensive. An alternative approach is to calculate the standard deviation of each error term independently and calculate the correlation matrix between these error terms. In this case, the total standard deviation is given by:

$$\sigma^2 \approx \sigma_{MRD}^2 + \sigma_{Vs}^2 + \sigma_{GM}^2 + 2\rho_{MRD,Vs}\sigma_{MRD}\sigma_{Vs} + 2\rho_{MRD,GM}\sigma_{MRD}\sigma_{GM} + 2\rho_{GM,V_s}\sigma_{GM}\sigma_{V_s} \tag{5}$$

Table 1 explains the notation for the components of the right hand side of Eq. (5). Table 1 also includes the simulation runs that are necessary to compute these terms. Note that Eq. (5) is expressed as an approximation rather than an equality because of the assumption underlying Eq. (4) (*i.e.*, that the contributions to Δ_{AF} can be separated additively). This assumption was verified for selected cases by running a simulation where all input parameters are randomized simultaneously. As indicated by Eq. (1), we assume that the uncertainty due to input motion and V_S variability (σ_{GM,V_S}) is computed separately and the effect of MRD uncertainty can be added to this uncertainty. Rearranging Eq. (1) we obtain:

$$\phi_{MRD} = \sqrt{\sigma^2 - \sigma_{GM,Vs}^2} \tag{6}$$

where σ^2 is estimated using Eq. (5). If some of the correlations in Eq. (5) are negative, the term inside the square root in Eq. (6) may be negative, in which case we assume simply that ϕ_{MRD} is equal to zero. As indicated before, we follow Rodriguez-Marek *et al.* [5] for the randomization of the V_S profile (which includes both randomization of the V_S values and the layer thicknesses) and the randomization of the input motion. In the following paragraphs, we discuss the randomization of MRD curves.

Table 1: Notation used Eq. (5) and an indication of the simulation runs used to compute the standard deviation components and their correlations. The correlation coefficients are computed assuming that the error components follow a multi-variate normal distribution.

Simulation runs	Parameters computed (Eq. 5)	Description
Randomize MRD curves and fix the input motion and V_S profile	σ_{MRD}	Standard deviation of AFs when only the input MRD curves are varied
Randomize V_S profiles and fix the input motion and MRD profile	σ_{V_S}	Standard deviation of AFs when only the input V_S profile is varied
Randomize input motion and fix the V_S profile and MRD curves	σ_{GM}	Standard deviation of AFs when only the input motion is varied
Randomize MRD curve and input motion and fix the V_S profile	$\sigma_{MRD,\mathrm{GM}}$	Standard deviation of AFs when MRD curves and input motion are varied
	$\rho_{MRD,\mathrm{GM}}$	Correlation between MRD and input motion error terms computed by: $$\rho_{MRD,\mathrm{GM}} = \frac{\sigma^2_{MRD,\mathrm{GM}} - \sigma^2_{MRD} - \sigma^2_{GM}}{2\sigma_{MRD}\sigma_{GM}}$$
Randomize V_S profile and input motion and fix the MRD curves	σ_{GM,V_S}	Standard deviation of AFs when V_S profile and input motion are varied
	ρ_{GM,V_S}	Correlation between V_S profile and input motion error terms computed by: $$\rho_{\mathrm{GM,V_S}} = \frac{\sigma^2_{GM,V_S} - \sigma^2_{V_S} - \sigma^2_{GM}}{2\sigma_{V_S}\sigma_{GM}}$$
Randomize V_S profile and MRD curves and fix the input motion	σ_{MRD,V_S}	Standard deviation of AFs when MRD curves and V_S profile are varied
	ρ_{MRD,V_S}	Correlation between Vs profile and MRD error terms computed by: $$\rho_{MRD,V_S} = \frac{\sigma^2_{MRD,V_S} - \sigma^2_{MRD} - \sigma^2_{V_S}}{2\sigma_{MRD}\sigma_{V_S}}$$

2.2.1 Generation of MRD curves

A methodology for the generation of MRD curves that are consistent with a statistical model of the uncertainty in MRD curves is needed for the simulations. We assume that each of the normalized shear modulus (MR) and damping values at a given strain level are log-normally distributed around a median value, and the MR and damping curves are mutually correlated. The ingredients needed for generating random MRD curves are a median and a standard deviation model for each of the MR and damping curves, and the correlation between damping and MR of each layer. Moreover, since MRD curves are generated for every layer in the site profile, an interlayer correlation for MR and damping curves is needed. In the remainder of this section, we introduce first the models adopted to estimate the mean and standard deviation of MRD curves. Then, we explain two necessary modifications to these curves. Finally, we discuss our choices for the interlayer and intralayer correlation of MRD curves and the sampling method used in the simulations.

We adopt the Darendeli [11] and Menq [12] models for the MRD curves. These authors proposed MRD curves for different soil types based on index properties and mean confining stresses. The different soil types encountered in the profiles analyzed in this paper are listed in Table 2. The Darendeli [11] model is used for all layers including clay, sandy clay, and clayey sand. This model is parameterized based on plasticity index (PI) and overconsolidation ratio (OCR). The Menq [12] model is used for sands and is parameterized using the grain size that corresponds to fifty percent of the sample passing by weight (D_{50}) and the coefficient of uniformity (C_u). The peat model presented in Rodriguez-Marek *et al.* [5] is used for peat layers. The deeper layers for all 19 zones are part of the Lower North Sea lithology (Kruiver *et al.* [9]). These materials are assumed to behave linearly with a damping of 0.5% (Rodriguez-Marek *et al.* [5]). Based on EPRI [13], damping of soil layers is limited to 15% as a conservative approach. The standard deviation of MRD values is obtained from a modified version of the Darendeli [11] model. While this model was developed specifically for the soils tested by Darendeli, we assume that the computed standard deviations are also applicable to other soil types. The Darendeli functional form for standard deviation of MRD curves is:

Table 2: Soil types in the Groningen field used in this study.

Soil type	OCR	K_0[a]	PI	Unit weight (kN)	C_u	D_{50} (mm)
Organic deposits(peat)	2 to 6	0.35-1.1	-	10.8-12	-	-
Clay	2 to 6	0.7-1.1	15-50	12.9-17.6	-	-
Clayey sand and sandy clay	2 to 6	0.5-1.4	30-50	16.8-18.1	-	-
Fine sand	1	0.5-1	0	18.3-19.7	1.76-5.53	0.08-0.13
Medium coarse sand	1	0.5	0	20.6-21	1.75-8.85	0.17-0.22
Coarse sand gravel and shells	1	0.5-1	0	20-21	1.74-12.34	0.23 - 0.47
Sand deep	1	1	0	21	2.61 - 4.08	0.156-0.25
Clay deep	2	1	30-40	21	-	-
Clayey sand deep	2	1	40	21	-	-
Lower North Sea Lithology	1	0.5	0	21	-	-

a) K_0 is the lateral earth pressure coefficient at rest and is used to compute mean confining stress

$$\sigma_{MR|PI} = e^{\,\varphi_{13}} + \sqrt{\frac{0.25}{e^{\,\varphi_{14}}} - \frac{(MR-0.5)^2}{e^{\,\varphi_{14}}}} \tag{7}$$

$$\sigma_{D|PI} = e^{\varphi_{15}} + e^{\varphi_{16}}\sqrt{D} \tag{8}$$

where MR is the ratio of shear modulus (G) over shear modulus at very low strains (G_{max}) and D is damping of soil in percent. The parameters φ_{13}, φ_{14}, φ_{15}, and φ_{16} are estimated by Darendeli [11] as -4.23, 3.62, -5 and -0.25, respectively. The left-hand side of Eqs. (7) and (8) indicates that these standard deviations are conditioned on a known value of PI. Equation (7) implies a non-zero value of standard deviation for MR at a strain of zero, which is physically inconsistent with the definition of MR. The approach adopted to deal with this issue is explained in the remainder of this section.

For the sites under analysis, the index parameters are estimated from a correlation with soil type and/or cone penetration test (CPT) tip resistance values. For this reason, the index parameters carry a considerable uncertainty (Kruiver *et al.* [9]). To accommodate this, we augment the MRD curves standard deviation to include this source of variability. We use a First Order Second Moment (FOSM) method to update the standard deviations to include the effect of uncertainty in index parameters. For example, to introduce the uncertainty into the computation of the standard deviation of MR curves, we use:

$$\sigma_{MR}^2 = (\sigma_{MR|PI})^2 + \left(\left|\frac{dMR}{dPI}\right|\sigma_{PI}\right)^2 \tag{9}$$

where σ_{MR}^2 is the unconditional uncertainty in MR and σ_{PI} is the standard deviation of PI. Equation (9) is first used to compute the σ_{MR} at the reference strain and then parameter φ_{14} in Eq. (7) is modified to fit this value. In this fashion the unconditional uncertainty at other strain levels can also be computed. The same process is used to include the uncertainty due to other soil index parameters.

The variability of damping also must be increased to account for the uncertainty in the soil parameters. To increase the variability in damping, first the standard deviation of damping is separated into the standard deviation of small strain damping ($Dmin$) and the remainder damping ($D - Dmin$) by:

$$\sigma_{D-Dmin}{}^2 = \sigma_D{}^2 - \sigma_{Dmin}^2 \tag{10}$$

where σ_D is the standard deviation of damping, and σ_{Dmin} is the standard deviation of damping at small strains, and σ_{D-Dmin} is the standard deviation of damping at strain γ minus damping at zero strain. Then the new standard deviations that incorporate the uncertainty in soil parameters are calculated based on the same method explained for the standard deviation of MR. Then new sets of φ_{15} and φ_{16} are calculated such that Eq. (8) gives the increased values for σ_{Dmin} and σ_{D-Dmin}. Figure 3 shows median of MR, median plus sigma when uncertainty in PI is not considered, and median plus sigma when uncertainty in PI is considered for one set of input parameters.

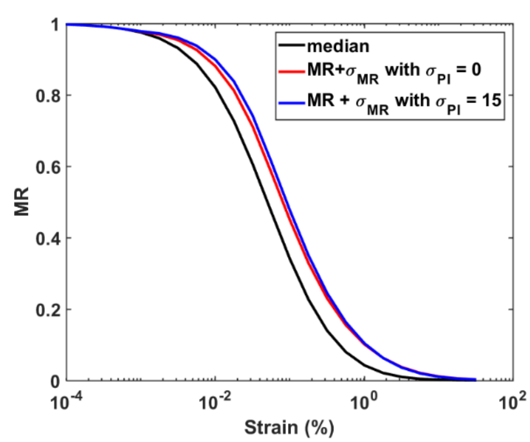

Fig. 3: Estimated MR of soil with PI = 10, OCR = 2 and mean effective pressure equal to 0.5 atm. The figure includes the median (black), median plus one standard deviation (red), and median plus one modified standard deviation (blue) curves

As mentioned previously, having uncertainty in MR at zero strain is not consistent with the definition of MR. To address this problem, the standard deviation of MR is set to be zero for strains lower than the elastic threshold strain defined by Vucetic and Dobry [14]. The threshold strain, which is a function of PI, is the strain level beyond which the soil starts to behave nonlinearly. For strains larger than the threshold strain, the standard deviation is increased from zero to its original value at a strain equal to 30 times the threshold strain. This method gives smooth realization of MR curves that approach one at very low strains.

An additional modification to Darendeli's model is that we assume a lognormal distribution for MR and damping values while Darendeli assumed a normal distribution. Using normal distribution for MR and damping values results in MRD curve randomizations that give negative MR at large strains or negative damping at small strains. We hence apply a transformation of the mean and standard deviation proposed by the Darendeli model to those of a log-normal distribution (Ang and Tang [15]). Figure 4a shows MR curve and MR plus and minus its standard deviation curve. Figure 4b shows the hysteresis loop for these three curves. A final modification to the curves is to modify the large strain portion of the MR curve such that the curves are consistent with the undrained strength of the soils. We use the approach of Yee *et al.* [16] for this purpose. We assume that the undrained strength of the soil is lognormally distributed, with a standard deviation of 0.5. Moreover, we assume that the undrained strength is fully correlated to the MR curves (implying that a random realization of an MR curve that lies above the median curve corresponds to a soil strength that is proportionally higher than its median value). Figure 5 shows MR curves corrected by different undrained strengths (S_u) and their corresponding hysteresis loops.

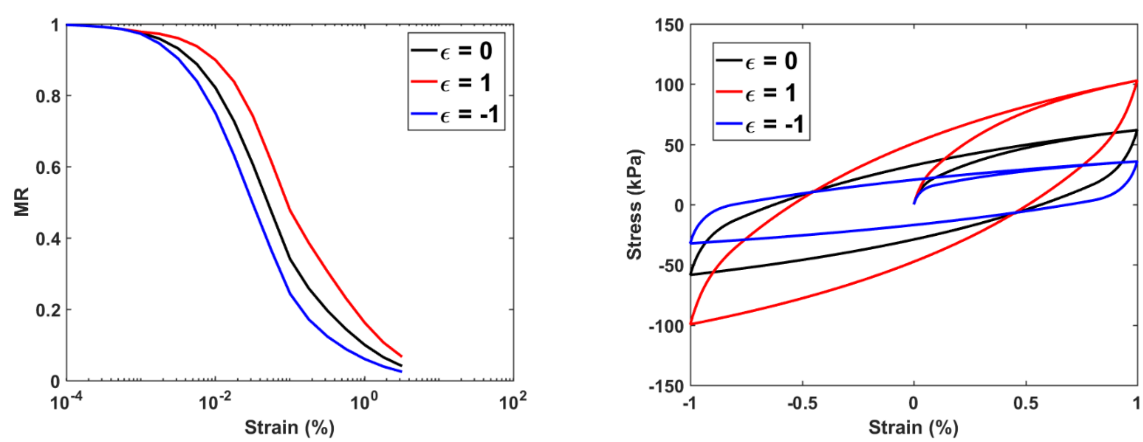

(a) (b)

Fig. 4: (Left) Estimated MR and (right) hysteresis loop of a soil with PI = 10, OCR = 2 and mean effective pressure equal to 0.5 atm. The figure includes the median (black), median plus one standard deviation (red), and median minus one standard deviation (blue)

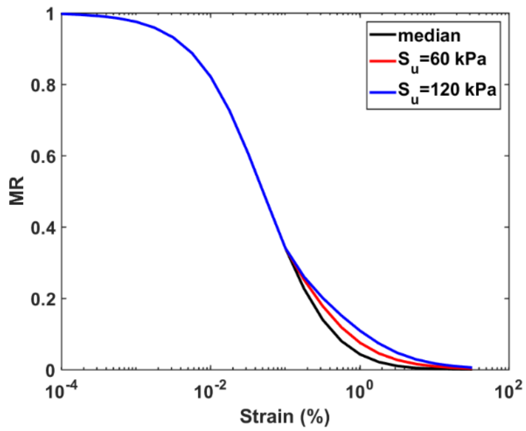

(a) (b)

Fig. 5 Comparison of MR curves (left) and hysteresis loops (right) that are corrected for different values of S_u

2.2.2 Correlation model

The Toro [17] methodology for producing randomized V_S profiles with layer-to-layer correlation is modified to produce randomized curves for shear modulus and damping. The randomized MR curve for layer *i*+1 is obtained by first computing the normalized deviation from the mean value:

$$\varepsilon_{i+1} = \sqrt{1 - \rho_{interlayer}^2}(\varepsilon_{i+1}^*) + \rho_{interlayer}\varepsilon_i \tag{11}$$

where ε_i is the normalized deviation from the mean used in producing the MR curve for layer *i*, ε_{i+1}^* is a random number taken from the standard normal distribution, and ε_{i+1} is the normalized deviation from the mean for layer i*+1*. This value is then used to calculate the MR value for layer i+1*:*

$$MR_{i+1} = e^{\mu_{\text{lnMR}} + \varepsilon_{i+1}\sigma_{\text{ln}MR}} \tag{12}$$

where the mean (μ_{lnMR}) and standard deviation (σ_{lnMR}) of MR are those that correspond to layer i+1. The procedure is modified to generate a realization of damping of layer i+1 (D_{i+1}) in order to account for the correlation of D_{i+1} with D_i and MR_{i+1}. This is accomplished by building a correlation matrix and then obtaining a modified normalized deviation from the mean (z_{i+1}) as follows:

$$A = \begin{bmatrix} A_{11} & A_{12} \\ A_{21} & A_{22} \end{bmatrix} = \begin{bmatrix} 1 & [\rho_{MR,D} \quad \rho_{interlayer}] \\ \begin{bmatrix} \rho_{MR,D} \\ \rho_{interlayer} \end{bmatrix} & \begin{bmatrix} 1 & \rho_{MR,D}\rho_{interlayer} \\ \rho_{MR,D}\rho_{interlayer} & 1 \end{bmatrix} \end{bmatrix} \quad (13)$$

$$z_{i+1} = z_{i+1}^{*}\sqrt{1 - A_{12} * A_{22}{}^{-1} * A_{21}} + A_{12} * A_{22}{}^{-1} \begin{bmatrix} \varepsilon_{i+1} \\ z_i \end{bmatrix} \quad (14)$$

$$D_{i+1} = e^{\mu_{\ln(Di+1)} + z_{i+1}\sigma_{\ln(Di+1)}} \quad (15)$$

where z_i is the normalized deviation from the mean used in producing D_i curve, z_{i+1}^{*} is a random number sampled from the normal distribution with zero mean and standard deviation one, z_{i+1} is the standardized error which is used to calculate the realized MR for layer *i*+1, and $\rho_{MR,D}$ is the correlation between MR and damping curves. Based on the recommendation of Kottke and Rathje [18], we assume this correlation to be equal to -0.5. The physical explanation for a negative correlation is that a lower MR curve than the median implies a higher degree of nonlinearity and consequently higher damping. We assume the MRD curves are fully correlated from layer to layer. This assumption decreases the required number of MRD curve realizations. In addition, preliminary results show that the assumption of full correlation of MRD curves leads to somewhat conservative results. This choice is desired given that no data are available to calibrate a layer-to-layer correlation model for the MRD curves. In the next section we examine the effects of this assumption.

2.2.3 Monte Carlo simulation approach

We follow the method proposed by Cools and Rabinowitz [19] to simulate a bi-normal distribution with a discrete number of points. These authors use nine pairs of numbers and corresponding weights to model a 2D Gaussian distribution. The selected weights are modified to account for the correlation between variables [19]. The nine points are presented in Table 3. Note that using this method requires having layers with fully correlated MRD curves.

Table 3: Nine-point discrete representation of 2D Gaussian distribution.

Point	$\boldsymbol{\varepsilon_G}$	$\boldsymbol{\varepsilon_D}$	$\boldsymbol{\varepsilon_D}$ **Corrected for** $\boldsymbol{\rho_{G,D} = -0.5}$	**Weight**
1	2	0	-1	0.0625
2	$\sqrt{2}$	$\sqrt{2}$	0.517638	0.0625
3	0	2	1.73205	0.0625
4	-$\sqrt{2}$	$\sqrt{2}$	1.93185	0.0625
5	0	0	0	0.5
6	-2	0	1	0.0625
7	-$\sqrt{2}$	-$\sqrt{2}$	-0.51764	0.0625
8	0	-2	-1.73205	0.0625
9	$\sqrt{2}$	-$\sqrt{2}$	-1.93185	0.0625

Figure 6 shows standard deviation of AFs that results from varying MRD curves for different interlayer correlations and sampling methods. The V_S profile is generated as described in (Kruiver *et al.* [9]). The line labelled "Partial Correlation" corresponds to using for the MRD curves the same interlayer correlation assumed in generating V_S profiles. These results were generated using 250 sets of MRD curves in the analyses. The line labelled "Full Correlation" corresponds to using full correlation (*i.e.*, $\rho_{interlayer} = 1$) between layers' MRD curves, and using a large set of samples (250) to capture the full MRD distribution. The line labelled "Full Correlation, 9-point discretization" corresponds to using full correlation between layers' MRD curves and the Cools and Rabinowitz [19] sampling method. Note that the σ_{MRD} calculated using the nine point discretization is not significantly different from the one computed using a large number of simulations, and in general it results in a slightly higher standard deviation. This methodology is adopted because it is computationally more efficient. Partial correlation reduces considerably the values of σ_{MRD}. This behavior is expected because full correlation magnifies the effect of deviations from the median, because they are then present in every layer.

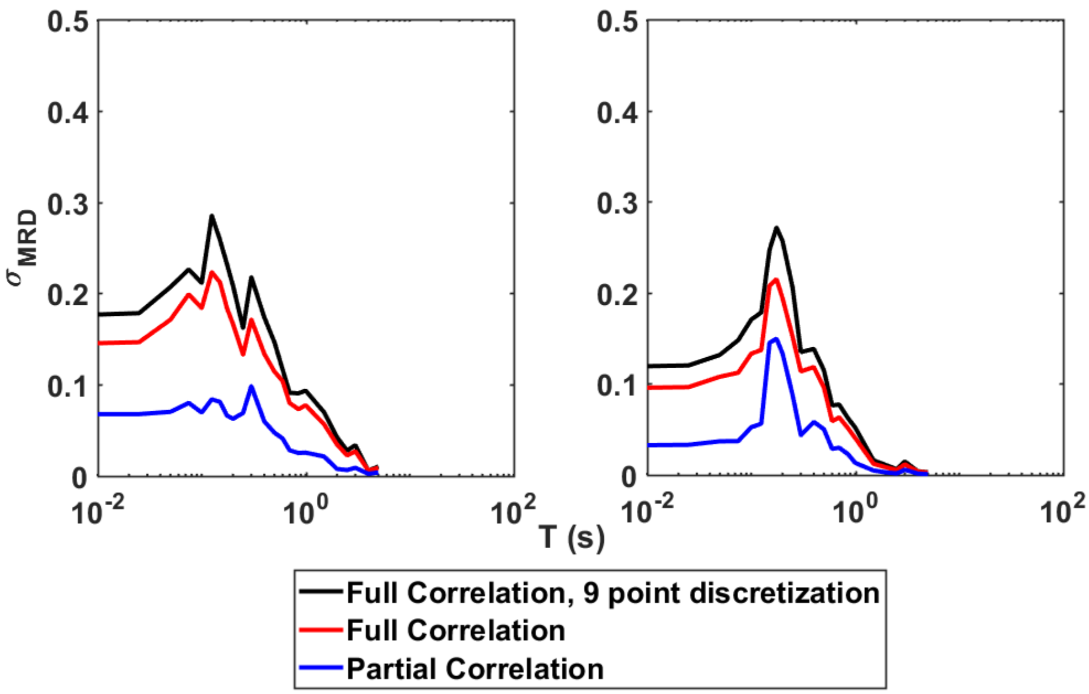

Fig. 6: Comparison of standard deviations corresponding to different interlayer correlation and sampling methods for Zones 620 (left) and 2047 (right)

3. Results

The methodology to compute the effects of varying MRD curves on the median and standard deviation was applied at a set of 19 representative zones in the Groningen field, chosen to sample the variation of lithology and stiffness encountered across the field. The selected zones are identified in Fig. 1. For each zone, 50 random V_S profiles are generated. The median V_S profiles of the selected zones are shown in Fig. 7, and selected site parameters are listed in Table 4. We use the same randomization scheme for shear-wave velocity profiles as described in (Kruiver *et al.* [9]). Amplification factors are computed for each of these profiles using equivalent linear analyses with the software ShakeVT2 (Lasley *et al.* [20]). A maximum likelihood regression is used to obtain the parameters for Eq. (2) and (3) for each zone and each oscillator period (an example of these fits is shown in Fig. 2). Following Rodriguez-Marek *et al.* [5], parameters S_{a1}, S_{a2}, and f_3 in Eq. (2) and (3) are fixed outside the regression. For consistency, we use the values for these parameters given in Rodriguez-Marek *et al.* [5]. The results are first presented in detail for zone 620. Then, the ϕ_{MRD} term (see Eq. 6) of all the selected zones are presented. Finally, a predictive model for the ϕ_{MRD} of these zones based on zone parameters is developed.

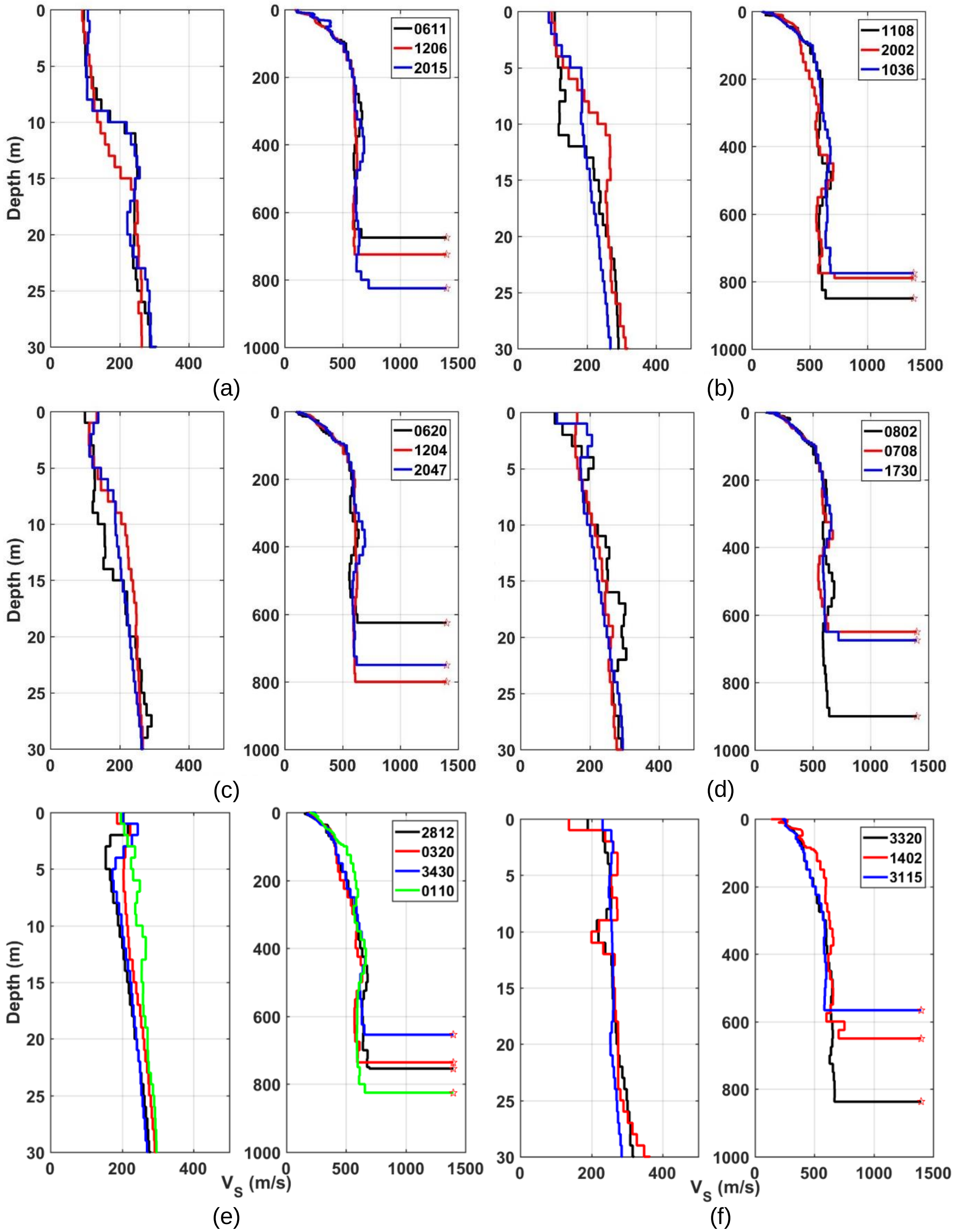

Fig. 7: Median V_S profile of the representative zones; for each plot, the detail of the uppermost 30 m is shown together with the full profile down to reference rock

Table 4: Site characteristics of each representative zone median profile. The description of soil types in the upper 30 m of median profile of each zone is provided in the electronic supplement.

Zone	V_{S5}(m/s)	V_{S10}(m/s)	V_{S30}(m/s)	Cumulative thickness of clay (m)	Maximum linear AF across all periods, max(f_1)
1730	174.1	177.9	226.9	78	1.03
2015	108.3	114.4	207.5	161	1.38
2047	122.4	148.0	201.2	182	1.30
110	216.3	228.2	258.4	170	0.861
611	98.7	117.4	207.0	98	1.32
620	115.9	122.0	193.0	125	1.29
802	151.3	171.4	239.3	287	0.976
1036	115.4	150.0	203.1	142	1.16
1108	110.0	117.74	203.7	233	1.29
1204	119.8	144.2	212.2	290	1.20
1402	236.6	246.1	266.6	73	0.865
708	160.7	174.6	226.4	145	1.05
1206	101.6	113.2	193.6	223	1.34
320	208.0	208.2	240.9	215	0.875
2002	110.8	150.2	231.5	187	1.13
2812	179.4	178.5	218.3	135	0.997
3115	251.7	252.1	260.6	187	0.782
3430	212.2	198.7	225.6	137	0.954
3320	231.8	238.1	263.7	180	0.824

The uncertainty in site properties has a clear impact on the uncertainty in AFs; however, it is also possible that uncertainty in site properties can have an effect on estimates of the median AFs. To evaluate this, we compute parameters f_1 and f_2 in Eq. (2) for zone 620 (Fig. 8). Note that f_2 does not change considerably as a result of the uncertainty of V_S and MRD. On the other hand, f_1 is affected, although the changes seen are relatively small. At small ground motion amplitudes (*i.e.*, low strains), the uncertainty in MRD results mostly from uncertainty in damping, and consequently f_1 is affected only at high frequencies. The effects of variability in V_S is to smooth f_1 across periods, as a result of each V_S profile randomization having a resonant period different from the resonant period of the median profile. Other authors (*e.g.*, Pehlivan *et al.* [21]) obtained similar results.

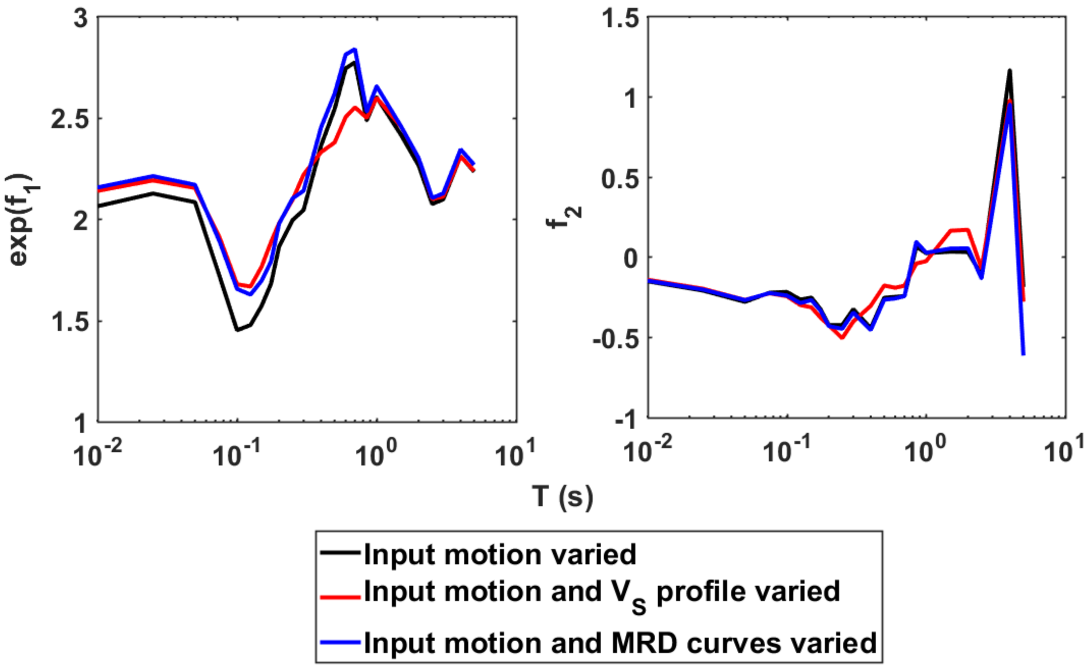

Fig. 8: Evaluating the effect of adding different source uncertainty on the parameters of the mean value of amplification function for zone 620. Note that exp(f_1) is used because this value corresponds to the linear AF (see Eq. 2)

The effect on standard deviations is computed separately for low-intensity motions and high-intensity motions. These two standard deviation components are then used to build a heteroskedastic model for standard deviation (Eq. 3). Figures 9a and 9b show the uncertainty components required for calculating σ (Table 1 and Eq. 5) for the low-intensity model for Zone 620, and Fig. 9c shows σ versus period for the same zone. Figure 9c implies that including MRD variability causes only a modest change in the standard deviation of the low-intensity model. The same behavior is observed for other zones. Observe in Fig. 9d that the effect of uncertainty in MRD on AFs standard deviation is small because low-intensity motions do not induce large strains and soil behavior remains linear. Figure 10 shows the components needed for calculating σ for the high-intensity model for the same zone. Because the motions corresponding to the high-intensity model induce large strains, adding uncertainty in MRD curves increases the standard deviation of AFs considerably (Figs. 10c and 10d).

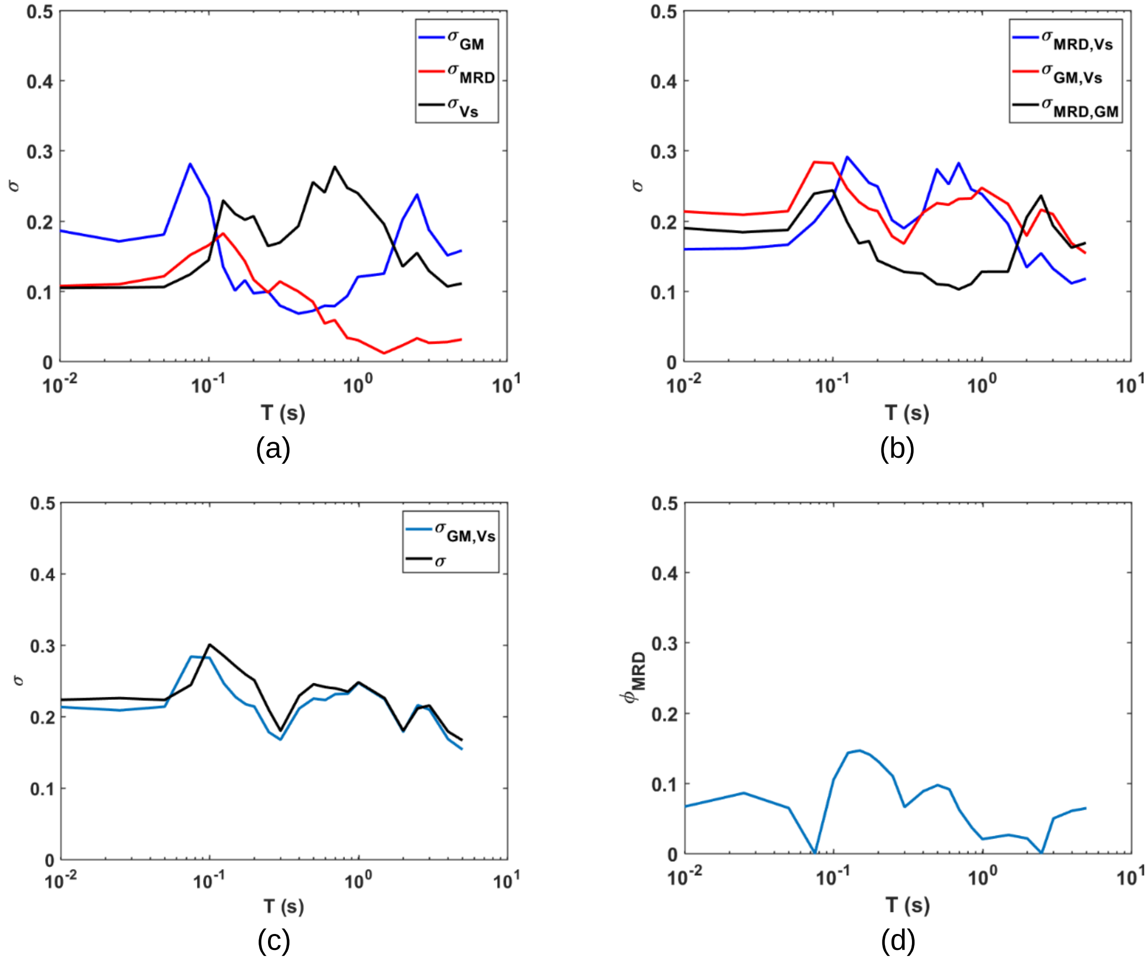

Fig 9: Different components of low-intensity model σ for Zone 620 (see Table 1 for notation)

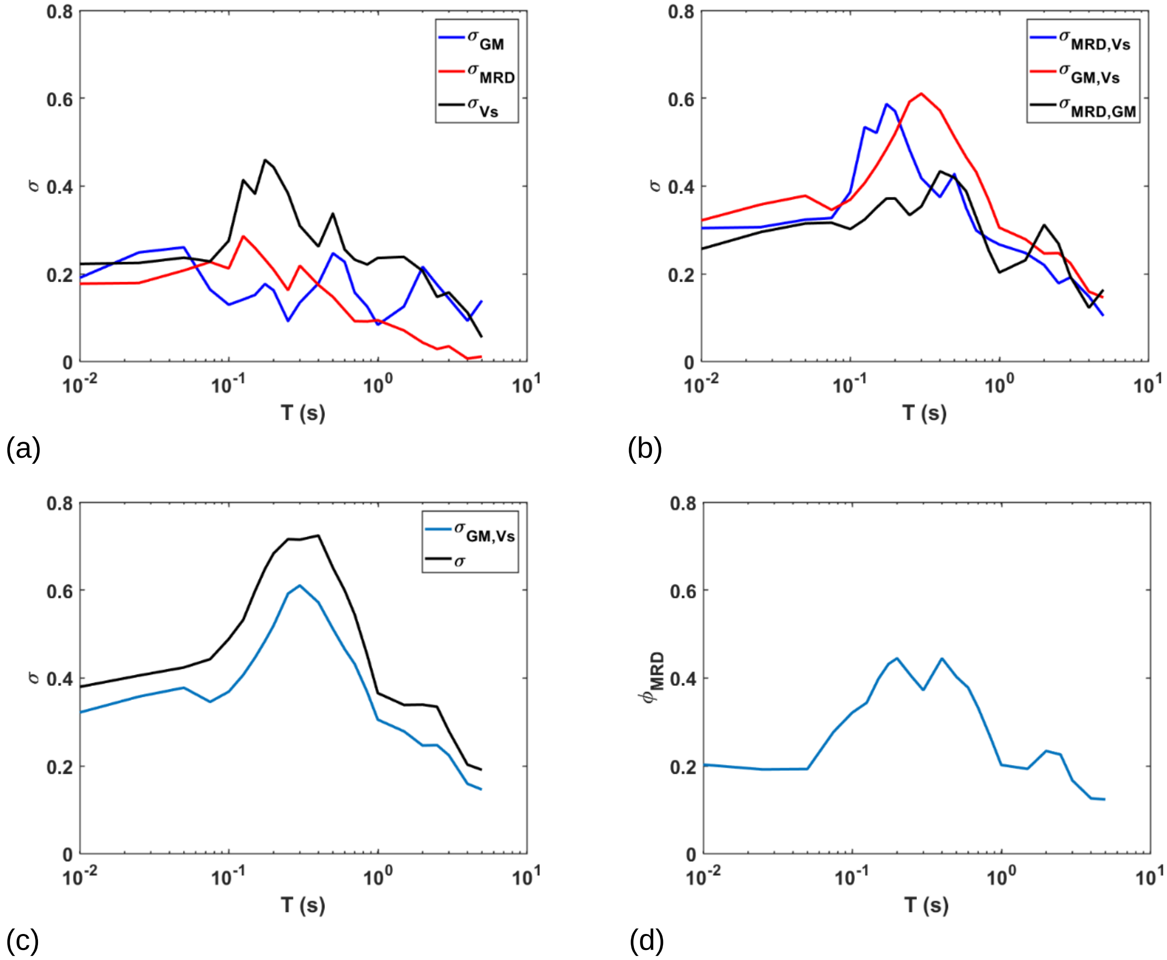

Fig. 10: Different components of high-intensity model σ for Zone 620 (see Table 1 for notation)

Figure 11 shows the effects of MRD uncertainty on the total AF uncertainty (*i.e.*, ϕ_{MRD}) versus period for the selected representative zones. For low-intensity motions, the contribution of MRD uncertainty is only significant (*i.e.*, larger than about 0.15 in natural log units) for oscillator periods slightly higher than 0.1 seconds. This seems to be consistent for all profiles, and reflects the periods that are more affected by small-strain damping. As expected, the effects of MRD uncertainty are more significant for high-intensity motions because the larger strains lead to nonlinear behavior. The effects of MRD uncertainty on AFs for large amplitude motions vary appreciably from zone to zone, implying that ϕ_{MRD} is highly site-dependent. This observation explains the differing observations of past studies (Rathje *et al.* [6]; Kwok *et al.* [7]; Li and Assimaki [8]). The values of ϕ_{MRD} vary from low (less than 0.2 across all periods) to extremely high for some profiles (above 0.5).

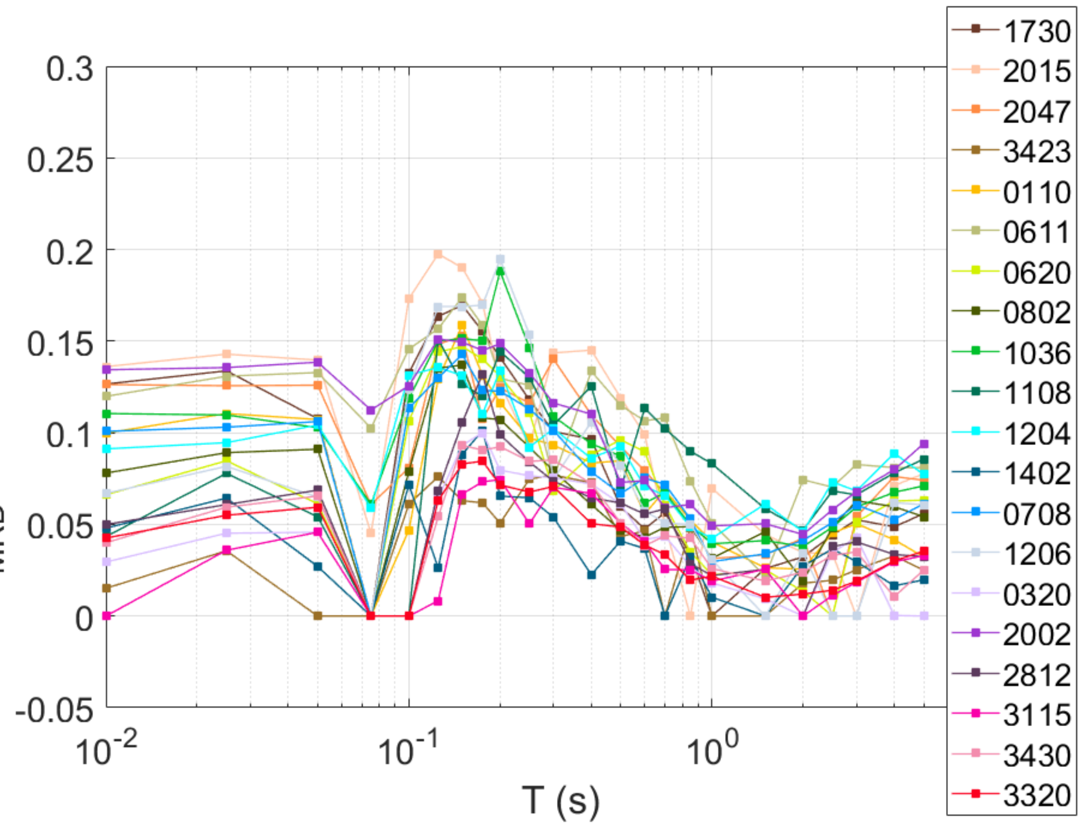

(a)

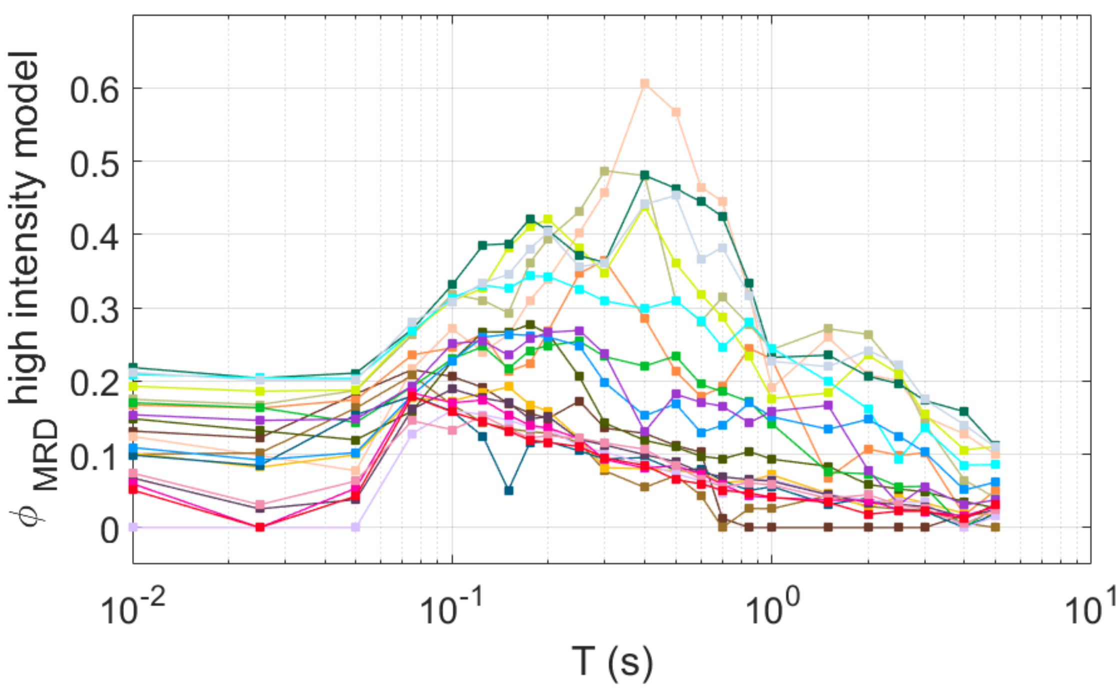

(b)

Fig. 11: ϕ_{MRD} vs period for (a) low-intensity and (b) high-intensity model versus for different zones

In order to generalize the results shown in Fig. 11, the values of ϕ_{MRD} must be correlated to site characteristics. In order to achieve this, we first develop a simplified representation for ϕ_{MRD} as shown in Fig. 12. For the low-intensity model, a tri-linear functional form is used. The limiting periods for this model are selected from a visual inspection of the curves shown in Fig. 11a. For the high-intensity model, a more complex shape is needed to fit the curves shown in Fig. 11b. This model reflects the fact that the values of ϕ_{MRD} are larger around the predominant period of each site. For this reason, the oscillator periods at which the ϕ_{MRD} model changes value vary from site to site.

The parameters in Figs. 12a and 12b are obtained for each of the zones in Fig. 11 as follows. For the low-intensity model, the parameters θ_1 and θ_2 are the mean (across period) of ϕ_{MRD} for periods lower than 0.5 s and larger than 1 s, respectively. For the high-intensity model, the parameter $T_{\theta 4}$ is the period at which ϕ_{MRD} is maximum; θ_4 is the mean (across period) of ϕ_{MRD} for periods between $e^{-0.4}T_{\theta 4}$ and $e^{0.4}T_{\theta 4}$; $T_{\theta 3}$ is equal to 0.05 s if $e^{-0.4}T_{\theta 4}$ is larger than 0.08 s and is equal to 0.025 s otherwise; and θ_3 and θ_5 are the mean high-intensity model of ϕ_{MRD} for periods smaller than $T_{\theta 3}$ and larger than 2 s, respectively. The constants $e^{0.4}$ and $e^{-0.4}$ indicate the length of the horizontal line in Fig. 12b, where $\phi_{MRD}$is equal to θ_4. The value of these constants were chosen based on observations and trial and error and were set to be equal for all zones.

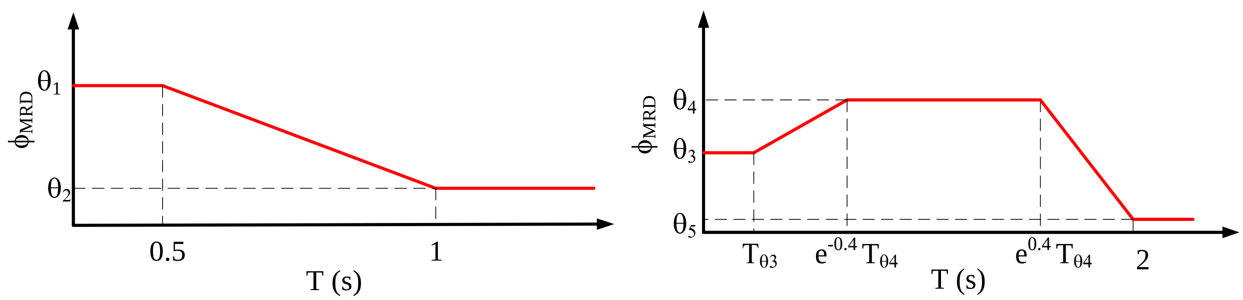

(a)

(b)

Fig. 12: Schematic illustration of (a) low-intensity ϕ_{MRD} and (b) high-intensity ϕ_{MRD} models

Once the parameters of the models in Fig. 12 are obtained for all the selected zones, these parameters are correlated to explanatory variables obtained from the average profile for each of the zones (Table 4); these correlations are listed in Table 5. The parameters of the low-intensity ϕ_{MRD} model correlate better with $V_{S,5}$. However, this parameter does not correlate as well with the high-intensity ϕ_{MRD} model. A parameter that works well for both the low-intensity and high-intensity models is the maximum value of linear AF across all periods (since the parameter f_1 corresponds to linear site response, we label this parameter $f_{1,max}$). This parameter is obtained from analyses where both V_S and input motion are randomized, but it can be obtained from a linear site response analysis of the mean profile for a site. The parameters of Fig. 12 are plotted versus $f_{1,max}$ (Fig. 13) and a simple model is fitted for each of these parameters.

Table 5: Correlation coefficients between the parameters of the ϕ_{MRD} model (Fig. 12) and site characteristics

Parameter	$\boldsymbol{\theta_1}$	$\boldsymbol{\theta_2}$	$\boldsymbol{\theta_3}$	$\boldsymbol{\theta_4}$	$\boldsymbol{\theta_5}$	T($\boldsymbol{\theta_4}$)
$V_{S,30}$	-0.711	-0.749	-0.723	-0.684	-0.589	-0.789
$V_{S,10}$	-0.785	-0.833	-0.862	-0.807	-0.763	-0.857
$V_{S,5}$	-0.832	-0.771	-0.825	-0.854	-0.837	-0.824
Cumulative thickness of clay layers	0.206	0.169	0.140	-0.0280	0.253	0.190
Cumulative thickness of layers with V_S less 100 m/s	0.497	0.433	0.415	0.486	0.388	0.493
$f_{1,max}$	0.802	0.866	0.910	0.810	0.730	0.900

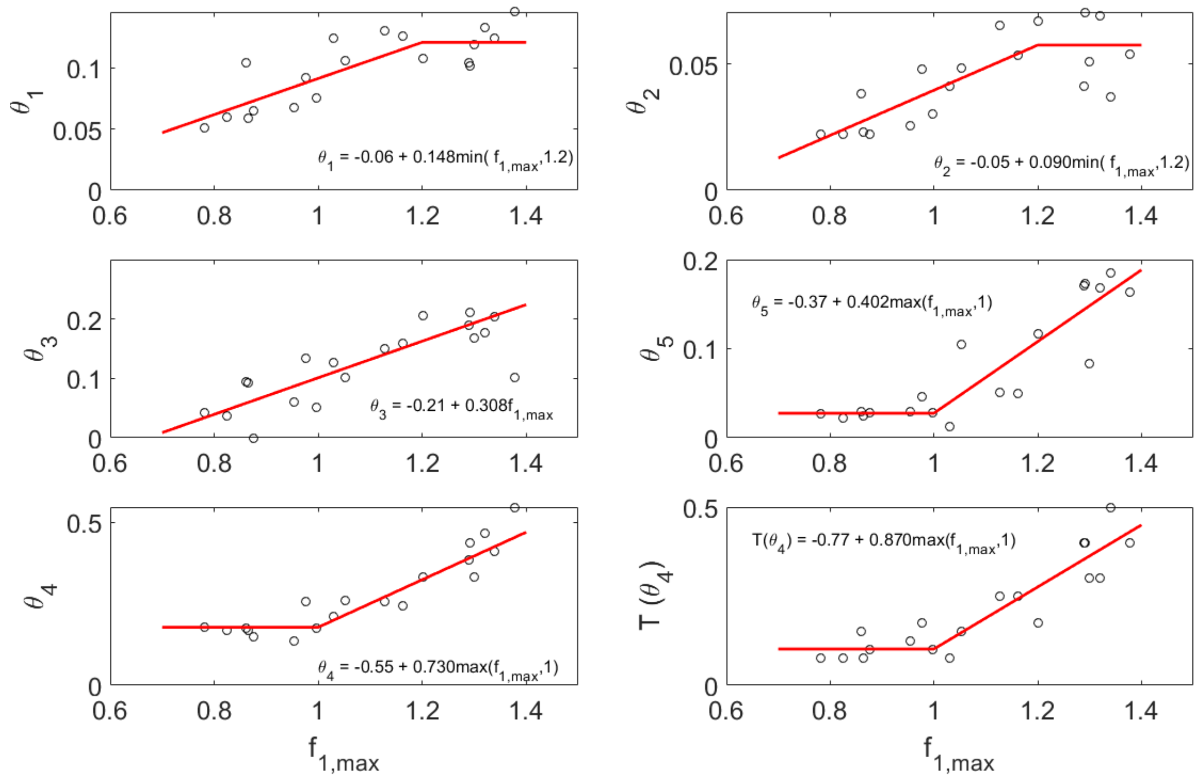

Fig. 13: Observed ϕ_{MRD} parameters versus $f_{1,max}$ for all zones (black circles). The red line is the prediction model for each parameter

Figure 14 shows the observed value of ϕ_{MRD} for Zone 620 along with its prediction based on the model in Fig. 12. A similar fit is seen for other zones. The models implicit in Fig. 13 are specific to the Groningen field; however, similar correlations should exist for other sites. Limited comparisons to sites in other regions have shown that the proposed model can be used as a first estimate of ϕ_{MRD} for soft and medium stiff sites in other locations. However, given the strong site dependency of ϕ_{MRD}, site-specific studies are generally recommended. In general, softer sites, which have stronger linear response, have higher values of ϕ_{MRD}, both for the low-intensity and high-intensity models. The periods over which the ϕ_{MRD} values are larger ($T_{\theta 4}$) also increases for softer sites.

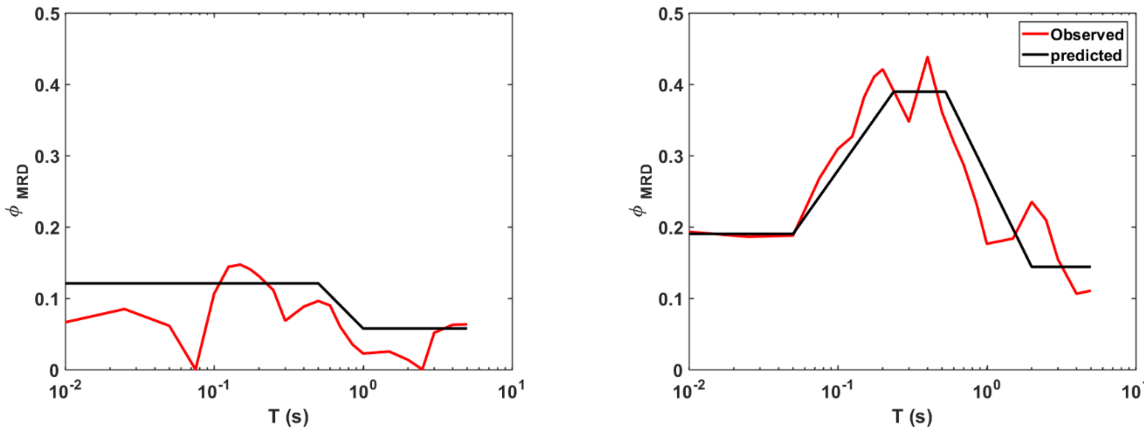

(a) (b)

Fig. 14: Predicted ϕ_{MRD} using the model in Fig. 13 along with observed $\emptyset_{\boldsymbol{MRD}}$ for zone 620. This zone has $f_{1,max}$ equal to 1.2893 (a) for low-intensity model and (b) for high-intensity model

4. Conclusions

This paper presented a study on how to capture the effects of the uncertainty of MRD curves on the uncertainty of the computed site amplification. A methodology is proposed wherein the effects of MRD uncertainty are computed without much additional computational cost to that associated with computing the effects of V_S uncertainty alone. The methodology is applied to a case history in the Groningen gas field in the Netherlands. The results show that the effect of uncertainty in MRD curves on standard deviation of $ln(AF)$ is highly dependent on soil profile. This effect can be significant for soft soils and strong input motions. Finally, we show that the effects of MRD uncertainty can be correlated to elastic site properties.

Acknowledgments

We are grateful to NAM for the support to conduct this work and particularly to Jan van Elk for leadership on the seismic hazard and risk assessment project within which this work was initially developed. We are also grateful to Pauline Kruiver and colleagues from Deltares for assistance with development of the soil profiles for Groningen. The Ph.D. studies of the first author are supported by Electricité de France under cooperation contract No. 3000-5910144023.

5. References

1. Bazzurro P, Cornell CA. Nonlinear soil-site effects in probabilistic seismic-hazard analysis. Bulletin of the Seismological Society of America. 2004;94(6):2110-23.

2. Rodriguez-Marek A, Rathje E, Bommer J, Scherbaum F, Stafford P. Application of single-station sigma and site-response characterization in a probabilistic seismic-hazard analysis for a new nuclear site. Bulletin of the Seismological Society of America. 2014;104(4):1601-19.

3. Bazzurro P, Cornell CA. Ground-motion amplification in nonlinear soil sites with uncertain properties. Bulletin of the Seismological Society of America. 2004;94(6):2090-109.

4. Bommer JJ, Stafford PJ, Edwards B, Dost B, van Dedem E, Rodriguez-Marek A, Kruiver P, van Elk J, Doornhof D, Ntinalexis M. Framework for a ground-motion model for induced seismic hazard and risk analysis in the Groningen gas field, The Netherlands. Earthquake Spectra. 2017;33(2):481-98.

5. Rodriguez-Marek A, Kruiver P, Meijers P, Bommer J, Dost B, van Elk J, Doornhof D. A regional site response model for the Groningen gas field. Bulletin of the Seismological Society of America. 2017; 107(5): 2067–2077.

6. Rathje EM, Kottke AR, Trent WL. Influence of input motion and site property variabilities on seismic site response analysis. Journal of Geotechnical and Geoenvironmental Engineering. 2010;136(4):607-19.

7. Kwok AO, Stewart JP, Hashash YM. Nonlinear ground-response analysis of Turkey flat shallow stiff-soil site to strong ground motion. Bulletin of the Seismological Society of America. 2008;98(1):331-43.

8. Li W, Assimaki D. Site-and motion-dependent parametric uncertainty of site-response analyses in earthquake simulations. Bulletin of the Seismological Society of America. 2010;100(3):954-68.

9. Kruiver PP, van Dedem E, Romijn R, de Lange G, Korff M, Stafleu J, Gunnink JL, Rodriguez-Marek A, Bommer JJ, van Elk J, Doornhof D. An integrated shear-wave velocity model for the Groningen gas field, The Netherlands. Bulletin of Earthquake Engineering. 2017; 15(9): 3555-3580

10. Stewart JP, Afshari K, Hashash YM. Guidelines for performing hazard-consistent one-dimensional ground response analysis for ground motion prediction. Pacific Earthquake Engineering Research Center, UC Berkeley, CA. 2014; PEER Rep. 2014/16.

11. Darendeli MB. Development of a new family of normalized modulus reduction and material damping curves. Dissertation, Department of Civil Engineering, University of Texas, Austin, TX. 2001

12. Menq F-y. Dynamic properties of sandy and gravelly soils. Dissertation, Department of Civil Engineering, University of Texas, Austin, TX. 2003

13. EPRI. Seismic Evaluation Guidance. Screening, Prioritization and Implementation Details (SPID) for the Resolution of Fukushima Near-Term Task Force Recommendation 2.1. Seismic. Electrical Power Research Institute, Palo Alto, California. 2013 February; EPRI Rep. No. 1025281

14. Vucetic M, Dobry R. Effect of soil plasticity on cyclic response. Journal of Geotechnical Engineering. 1991;117(1):89-107.

15. Ang AH-S, Tang WH. Probability concepts in engineering planning and design: Basic principles (Volume I). New York, NY: Wiley; 1984.

16. Yee E, Stewart JP, Tokimatsu K. Elastic and large-strain nonlinear seismic site response from analysis of vertical array recordings. Journal of Geotechnical and Geoenvironmental Engineering. 2013;139(10):1789-801.

17. Toro G. Probabilistic models of site velocity profiles for generic and site-specific ground-motion amplification studies. Brookhaven National Laboratory, Upton, N.Y. 1995; Technical Rep. No. 779574,

18. Kottke AR, Rathje EM. Technical manual for Strata. Pacific Earthquake Engineering Research Center, Berkeley, California. 2009; Rep. No. 2008/10,

19. Cools R, Rabinowitz P. Monomial cubature rules since “Stroud”: a compilation. Journal of Computational and Applied Mathematics. 1993;48(3):309-26.

20. Lasley S, Green R, Rodriguez-Marek A. Comparison of equivalent-linear site response analysis software. Proc., 10th US National Conf. on Earthquake Engineering, Earthquake Engineering Research Institute, Oakland, CA; 2014

21. Pehlivan M, Rathje EM, Gilbert RB. Factors influencing soil surface seismic hazard curves. Soil Dynamics and Earthquake Engineering. 2016;83:180-90.